Journal of ELECTRONIC MATERIALS, Vol. 42, No. 4, 2013
DOI: 10.1007/s11664-012-2452-4

Corrosion Behavior of Pb-Free Sn-1Ag-0.5Cu-*X*Ni Solder Alloys in 3.5% NaCl Solution

UDIT SURYA MOHANTY[1,2] and KWANG-LUNG LIN[1,3]

1.—Department of Materials Science and Engineering, National Cheng Kung University, Tainan, Taiwan, ROC. 2.—e-mail: suryaudit@yahoo.com. 3.—e-mail: matkllin@mail.ncku.edu.tw

Potentiodynamic polarization techniques were employed in the present study to investigate the corrosion behavior of Pb-free Sn-1Ag-0.5Cu-*X*Ni solder alloys in 3.5% NaCl solution. Polarization studies indicated that an increase in Ni content from 0.05 wt.% to 1 wt.% in the solder alloy shifted the corrosion potential (E_{corr}) towards more negative values and increased the linear polarization resistance. Increased addition of Ni to 1 wt.% resulted in significant increase in the concentration of both Sn and Ni oxides on the outer surface. Secondary-ion mass spectrometry and Auger depth profile analysis revealed that oxides of tin contributed primarily towards the formation of the passive film on the surface of the solder alloys containing 0.05 wt.% and 1 wt.% Ni. Scanning electron microscopy (SEM) and energy-dispersive x-ray spectroscopy (EDX) established the formation of a Sn whisker near the passive region of the solder alloy obtained from the polarization curves. The formation of Sn whiskers was due to the buildup of compressive stress generated by the increase in the volume of the oxides of Sn and Ni formed on the outer surface. The presence of Cl^- was responsible for the breakdown of the passive film, and significant pitting corrosion in the form of distinct pits was noticed in Sn-1Ag-0.5Cu-0.5Ni solder alloy after the polarization experiment.

Key words: Corrosion, Pb-free solder alloy, polarization, passivity, pitting, SIMS

INTRODUCTION

Due to the inherent toxicity of Pb-containing compounds, there has been a worldwide effort to eliminate Pb-containing solders from the electronics industry. Also, increased health concerns over the use of lead present in eutectic Sn-Pb solders have promoted the development of new lead-free solders for microelectronic packaging.[1–3] Among the new lead-free solders, the new eutectic Sn-Ag-Cu (SAC) solder alloys have been the most promising candidates for replacement of Pb-containing solders in packaging and interconnect applications.[4–6] The advantages of this alloy system over the Sn-Ag binary eutectic alloy are its superior mechanical properties, relatively low melting temperature, and good solderability.[7] Addition of copper also enhances the corrosion resistance of Sn-Ag solder alloys, which exhibit improved passivity behavior compared with $Sn_{73.9}Pb_{26.1}$ solder.[8] With the development of surface-mount technology and the popular trend towards ultrafine-pitch designs, it has become imperative to develop new lead-free solders with improved mechanical properties.[9] To further enhance the properties of SAC solder alloys, alloying elements such as Bi, Sb, Sn, and Ni have been added to these alloys.[10,11] Wang et al.[12] observed that addition of Ni to SAC solders retarded Cu_3Sn growth and also changed the microstructure of the Cu_6Sn_5 compound formed near the interface. Dudek et al.[13] observed that addition of a small amount of rare-earth (RE) elements improved the reliability of SAC solder joints. Wang[14] found that addition of a trace amount of the RE cerium (Ce) also had a significant effect on the properties of SAC solder, such as the wetting, microstructure, creep behavior, and tensile properties of solder joints. Kim et al.[15] reported that

(Received July 6, 2012; accepted December 28, 2012; published online February 21, 2013)

addition of a small amount of nickel into Sn-*X*Ag-0.5Cu (*X* = 1 to 2) solders improved their mechanical properties, especially for solder bumps with several hundred diameters. Regarding the corrosion behavior of SAC solder alloys in chloride solution, very few studies have been carried out. Rosabino et al.[16] reported the corrosion behavior of Sn-3Ag-3Cu (at.%) alloys in 0.1 M NaCl solution by potentiodynamic polarization and impedance spectroscopy measurements. They observed that Sn-3Ag-3Cu solder alloy exhibited better corrosion behavior than Sn-3Ag-0.5Cu solder and attributed this to the presence of a more adherent and compact surface film of corrosion products. Song and Ricky Lee[17] observed that Sn-4Ag-0.5Cu lead-free solders corroded more easily than Sn-37%Pb solder balls when subjected to the salt-spray test.

The electrochemical corrosion behavior of Pb-free Sn-8.5Zn-0.05Al-*X*Ga and Sn-3Ag-0.5Cu alloys based on potentiodynamic polarization techniques was reported in our previous study.[18] A significant increase in the corrosion rate and corrosion current density of Sn-3Ag-0.5Cu alloy was observed as compared with the four-element alloys. Nevertheless there has not been any investigation on the corrosion behavior of SAC solder alloys containing Ni as an additional element. The reliability of SAC solder can be improved by doping with minor elements. Ni doping of SAC solder can reduce the interfacial reaction and suppress the Kirkendall voids. The presence of additives such as Ni, Ge, and Bi[19] in Pb-free solders also introduced certain properties which helped in controlling the grain structure and also reduced the degree of Cu dissolution in the solder. Also, solder alloys with lower Ag content, especially 1 wt.%, are employed from the viewpoint of material cost, because silver is one of the more expensive raw materials.

Based on these advantages of Ni addition to Pb-free solder, in this work an attempt is made to investigate the electrochemical corrosion behavior of Sn-1Ag-0.5Cu-*X*Ni solder alloys in 3.5% NaCl solution. Sn whisker formation after anodic polarization of the solder at certain specific potentials is also examined.

EXPERIMENTAL PROCEDURES

Alloys of Sn, Ag, Cu, and Ni were prepared from pure elements. The Ni content in the Sn-1Ag-0.5Cu-*X*Ni solder alloy varied from 0.05 wt.% to 1 wt.%. The preparation of Sn-1Ag-0.5Cu-*X*Ni solder alloy was accomplished by employing the methods used in our previous study.[20] The alloy thus formed after cooling was polished with SiC paper of grit 240, 800, 1200, and 2000, respectively, rinsed with distilled water, followed by cleaning in an ultrasonic cleaner. Potentiodynamic polarization tests were conducted in a rectangular cell[21] to investigate the corrosion behavior of the Sn-1Ag-0.5Cu-*X*Ni solder alloys in 3.5% NaCl solution. The scan rate for the polarization experiments was maintained at 1 mV/s, and polarization curves were recorded in the potential range of −1200 mV to +100 mV. A Pt wire was used as the counterelectrode, and a Ag/AgCl electrode saturated with KCl was employed as the reference electrode. The details of the polarization studies are reported in our previous study.[21] The elemental composition of the oxide layer and various corrosion products was determined by Auger electron spectroscopy (AES). Auger spectra were analyzed using a primary electron beam of magnitude 10 keV and 0.1 mA. Sputter depth profiles were obtained using a differential pumped ion gun with an ion beam accelerated at 3 keV. The sputtering rate was calibrated to 0.1 nm/s by etching a Si sample covered with SiO_2 film of known thickness. The secondary-ion mass spectrometry (SIMS) technique was used in our present study to identify the localized distribution of individual elements as well as associations of these elements. Such localized distribution can be measured in all three dimensions by virtue of the depth profiling capability of SIMS. The composition of the surface of the passive film and its underlying layer can be determined by SIMS depth profile analysis using the CS^+ microbeam energy of 10 keV. A primary ion beam of CS^+ with 50 nA beam current was rastered over an area of 150 μm × 150 μm on the specimen surface. The resultant intensity of the secondary ions was plotted versus the sputtering time to understand the variations in the composition of the various elements distributed across the modified layer.

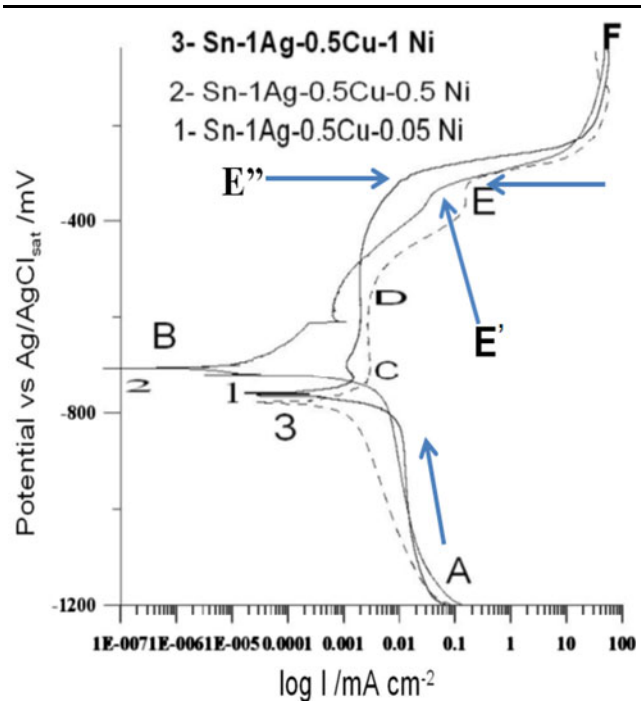

Fig. 1. Potentiodynamic polarization curves for Sn-1Ag-0.5Cu-*X*Ni solder alloys with various Ni contents in 3.5% NaCl solution.

RESULTS AND DISCUSSION

Polarization Studies

Figure 1 presents a semilogarithmic plot for the four-element Sn-1Ag-0.5Cu-*X*Ni solder with various Ni contents obtained in 3.5% NaCl solution. The anodic polarization part in Fig. 1 consists of several regions, named AB, BC, CD, DE, and EF. Since all the corrosion tests were performed in aerated NaCl solution, the cathodic branch of the polarization curves (region AB) may be ascribed to the dissolved oxygen reduction reaction as reported earlier:[22]

$$O_2 + 2H_2O + 4e^- \rightarrow 4OH^-. \quad (1)$$

It can be noted from curve 1 in Fig. 1 that there is a rapid increase in current with further scanning of the potential in the anodic direction, resulting in the formation of a sharp peak. The sharp peak obtained at B may be attributed to active dissolution of Sn during polarization of Sn-1Ag-0.5Cu-0.05Ni solder alloy to −750 mV. The results suggest that tin (Sn) present in the above solder takes priority in dissolution. Region BC in the polarization curve corresponds to increased dissolution of Sn with increasing potential in the anodic direction.

Anodic dissolution of tin is associated with active dissolution of Sn to Sn^{2+} and Sn^{4+}[23,24]

$$Sn \rightarrow Sn^{2+} + 2e^- \quad \left(E^0_{Sn^{2+}/Sn^0} = -0.136\ \text{V/NHE}\right), \quad (2)$$

where $E^0_{Sn^{2+}/Sn^0}$ refers to the standard oxidation potential at 298 K.

This reaction is followed by the formation of Sn^{4+} species as follows:

$$Sn^{2+} \rightarrow Sn^{4+} + 2e^- \quad \left(E^0_{Sn^{4+}/Sn^{2+}} = 0.151\ \text{V/NHE}\right). \quad (3)$$

The dissolution of Sn is also affected by the presence of other elements in the solder alloy. Since the electrode potential of Ag (0.7996 V) is higher than that of Sn (−0.1375 V), dissolution of tin into the corrosive solution is induced when these two metals are present in the solder alloy. Also, previous studies[25] have reported that the presence of Ag_3Sn in SAC solders would accelerate the dissolution of tin due to galvanic corrosion.

Point B in Fig. 1 is referred to as the corrosion potential (E_{corr}), where the extrapolated anodic and cathodic Tafel slopes intersect and the current becomes zero. A shift in the corrosion potential (E_{corr}) towards more negative values (Fig. 2a) is observed with increase in the Ni content from 0.05 wt.% to 1 wt.%, indicating an increase in the dissolution of tin with increasing nickel content. These changes are also reflected in the linear polarization resistance (LPR) values of the polarized solder. The LPR value was calculated by computer simulation using new ACM software, and the values are plotted in Fig. 2b. The LPR value undergoes an increase as compared with 0.5 wt.% Ni with increase in the Ni content to 1 wt.%. Higher LPR values correspond to lower corrosion rates.[26] Hence, an increase in the Ni content to 1 wt.% in the Sn-1Ag-0.5Cu-*X*Ni solder results in increased corrosion resistance due to minimum corrosion. The dissolution of tin continues with increasing potential until the hydroxide/oxide concentration reaches a critical value at point C (−700 mV, curve=1, Fig. 1). The current observed at this point is maximum and is referred to as the critical current density; the potential at this point is termed the passivation potential (E_{pp}). The supersaturation of oxides of tin at point C is clearly observed in the SEM micrographs (Fig. 3a, b) and also confirmed by EDX analysis.

Formation of oxides of Sn(II) and Sn(IV) might take place through the following equations:[27]

$$2Sn + O_2 + 2H_2O \rightarrow Sn(OH)_2. \quad (4)$$

$Sn(OH)_2$ easily dehydrates to form SnO

$$Sn(OH)_2 \rightarrow SnO + H_2O. \quad (5)$$

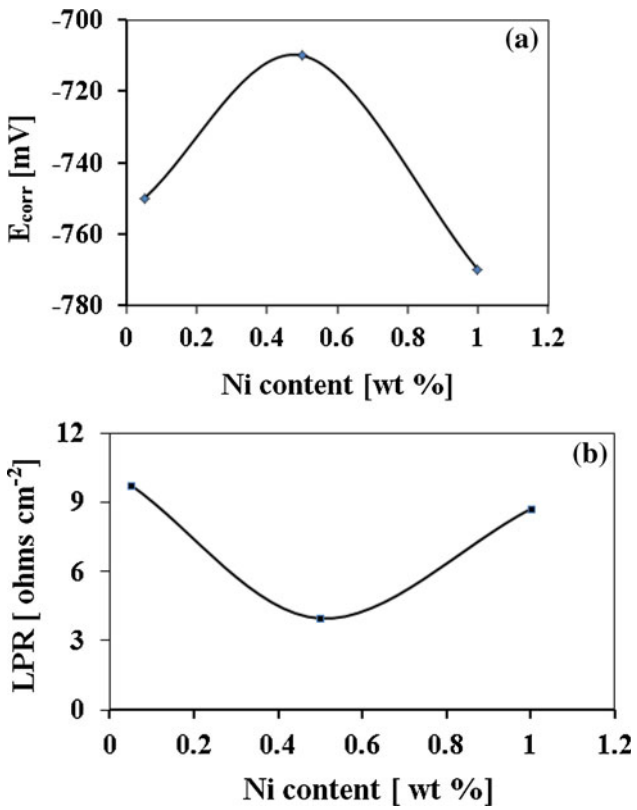

Fig. 2. Plot of Ni content (wt.%) versus (a) E_{corr} and (b) LPR values obtained after polarization of Sn-1Ag-0.5Cu-*X*Ni solder in 3.5% NaCl solution.

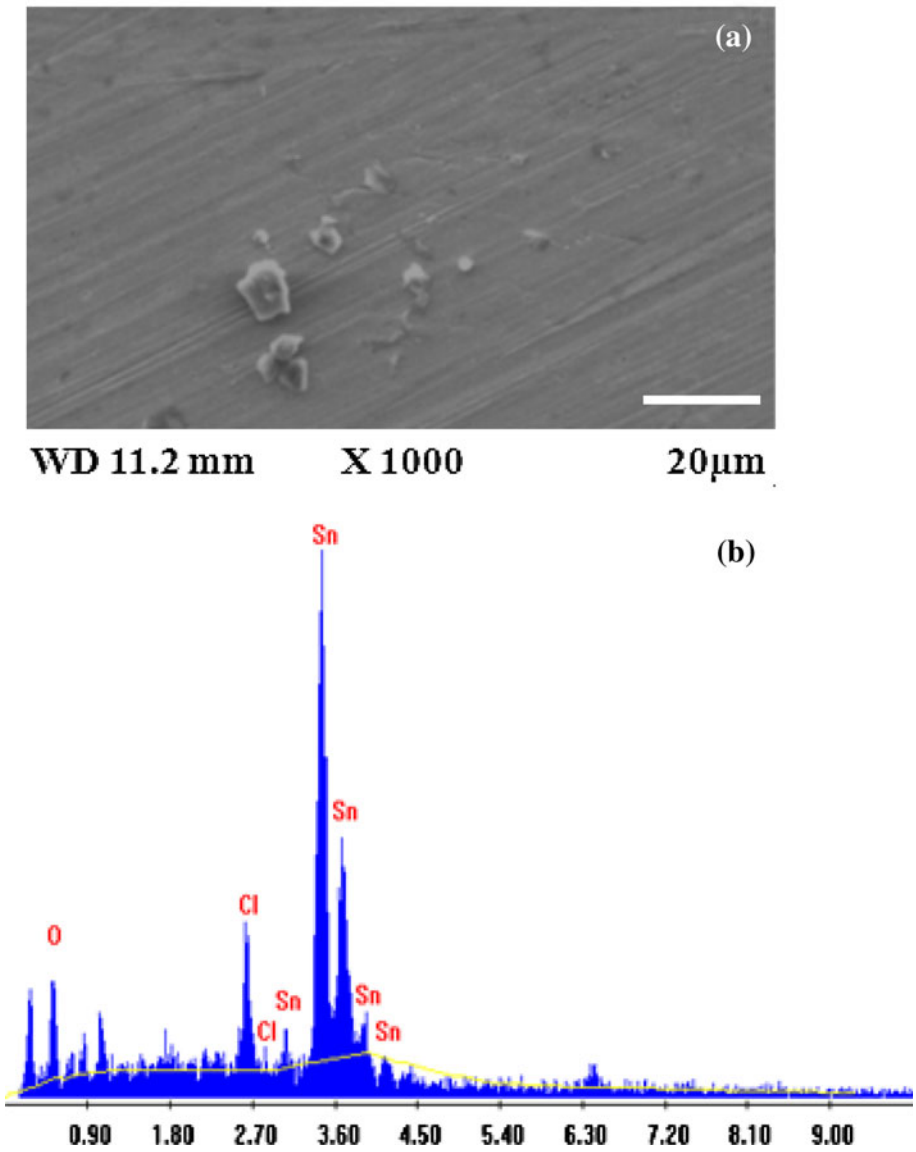

Fig. 3. (a) SEM micrograph for Sn-1Ag-0.5Cu-0.05Ni solder alloy polarized to point C during anodic excursion of the potential scan from −1200 mV to +100 mV and (b) EDX spectrum.

Further oxidation of SnO to stannic hydroxide $[Sn(OH)_4]$[28] may partially hydrate to stannic oxide (SnO_2) as shown in the reactions below:

$$SnO + 2OH^- + H_2O \rightarrow Sn(OH)_4 + 2e^- \quad (6)$$

$$Sn(OH)_4 \rightarrow SnO_2 \cdot H_2O + H_2O. \quad (7)$$

$Sn(OH)_4$ is highly insoluble and precipitates, giving rise to a more protective passivating film whose stability increases with the dehydration reaction.[29]

Hence, from the above equations, the formation of SnO and SnO_2 species is thermodynamically favored. Beyond the passivation potential, the active dissolution current density falls rapidly to a very small value, indicating the onset of permanent passivation. The value in this region, extending from C to D with almost constant current density, is referred to as the passivation current density. It can be noticed from Fig. 1 that, among the three investigated solder alloys, the current density remains independent of potential over a range of about 200 mV for Sn-1Ag-0.5Cu-0.05Ni solder (curve 1) and around 180 mV for Sn-1Ag-0.5Cu-1Ni (curve 3) as compared with Sn-1Ag-0.5Cu-0.5Ni (curve 2). These results indicate that Sn-1Ag-0.5Cu-0.05Ni and Sn-1Ag-0.5Cu-1Ni solder alloys demonstrate better passivation abilities and better corrosion resistance properties than the solder alloy containing 0.5 wt.% Ni. Certain assumptions can be made regarding the passivation of Sn-1Ag-0.5Cu-0.05Ni

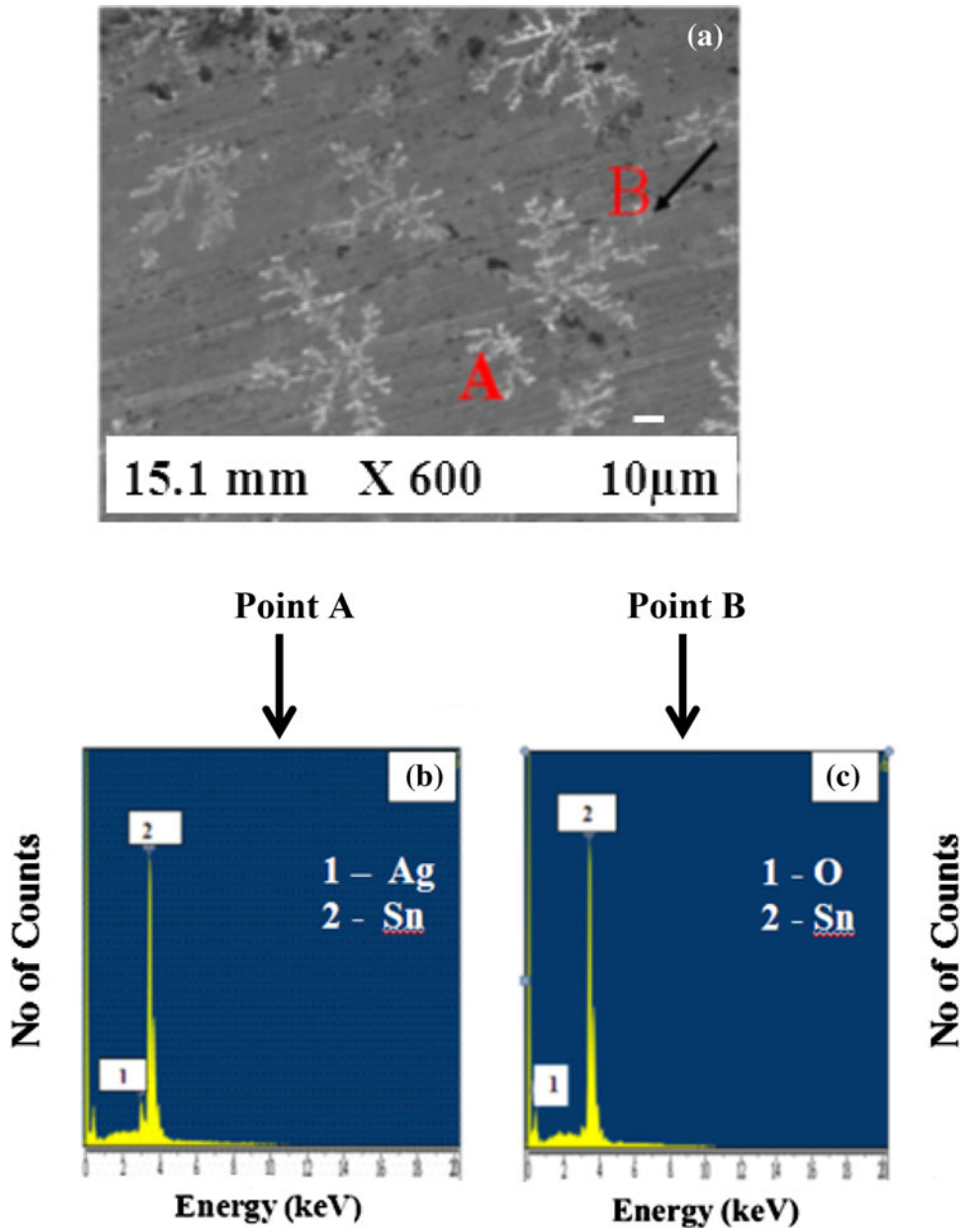

Fig. 4. (a) SEM micrograph for Sn-1Ag-0.5Cu-0.05Ni solder alloy polarized to point D during the anodic excursion of the potential scan from −1200 mV to +100 mV, (b) EDX spectrum, point A and (c) EDX spectrum, point B.

solder alloy; i.e., the less noble component of the alloy (Sn) might oxidize first, leading to a passivating tin oxide layer. This partially protective layer might inhibit silver dissolution from the alloy. Ag_3Sn on the other hand might contribute towards the passivation behavior of Sn-1Ag-0.5Cu-0.05Ni solder alloy. The micrographs in Fig. 4a show a finer, dendrite-like morphology for Ag_3Sn particles. EDX analysis also established the formation of Ag and Sn on the surface of the solder matrix (Fig. 4b, c). Garcia et al.[30] have demonstrated that, since the Ag_3Sn intermetallic is nobler than both the β-Sn matrix and the Sn-rich phase in the eutectic mixture, fiber-like Ag_3Sn particles envelope the Sn-rich phase (less noble region), providing corrosion protection, when the finer dendrite arm spacing is more homogeneously distributed.

Further scanning of the potential in the anodic direction starting from D results in the formation of a plateau within −350 mV to −300 mV at point E for the solders containing 0.5 wt.% and 1 wt.% Ni. Similar peaks have been observed[31] at around the same potential while investigating the passivation and pitting corrosion of nanostructured Sn-Ni alloys in NaCl solution; they were attributed to anodic dissolution of nickel present in the alloy and its transformation to NiO. Dissolution of Ni occurred according to the following reactions:[32]

$$Ni + OH^- \rightarrow NiOH^+ + e^- \quad (8)$$

$$NiOH^+ \rightarrow NiO + H^+. \quad (9)$$

Our results are also consistent with the data reported by several authors.[33,34] The plateau formation seems to be more predominant in the case of Sn-1Ag-0.5Cu-1Ni solder as compared with other solders containing 0.05 wt.% (curve 1) and 0.5 wt.% Ni (curve 2), suggesting that higher Ni content in the solder alloy led to higher concentration of NiO. Beyond point E, a rapid increase in current occurs (Fig. 1) with increase in anodic potential. This potential is referred to as the pitting potential (E_{pit}) or the transpassive potential. The pitting potential can also be assessed as the potential at which a consistent increase in current density occurs, indicating the initiation of nonpassivating pits. The pitting behavior of Sn-1Ag-0.5Cu-0.5Ni solder alloy in region EF is demonstrated in the SEM micrograph (Fig. 5). The pits (Fig. 5) formed on the surface of the solder alloy are found to be distinct and spherical. The pitting attack is more predominant in Sn-1Ag-0.5Cu-0.5Ni solder alloy as compared with other investigated solder alloys on the basis of the negative E_{pit} value (−340 mV) exhibited by Sn-1Ag-0.5Cu-0.5Ni solder alloy as compared with the noble E_{pit} values of −320 mV and −300 mV, respectively, for solders containing 0.05 wt.% and 1 wt.% Ni, respectively, as marked by arrows in Fig. 1. The occurrence of pit initiation at transpassive potentials can be rationalized in terms of localized breakdown of a surface film that is somewhat less protective than that prevalent in the passive region. Vetter and Strechblow[35] documented the occurrence of a salt layer within the pits at higher anodic potentials. Another assumption made by the authors is that the breakdown of the passivation film either could have been caused by the existence of Cl^- adsorbed by the corrosion products or be due to the oxygen evolution reaction. This is supported by reports by Smialowska[36] that a majority of construction materials in the industry suffer from pitting only in solutions containing or other halogen ions. Three main reasons are cited for the specific effects of chloride and its ability to produce pitting: (1) formation of a complex with cation and hydroxide, (2) increasing the activity of hydrogen ions in the pit electrolyte, and (3) forming a salt layer at the bottom of pits. The third factor appears to explain the specific role of halides in the pitting attack. It is suggested that the transition from passivity to the pitting condition can be explained by a competitive adsorption mechanism[37,38] in which chloride ions move into the double layer (oxide/liquid interface) of the electrode surface, eventually reaching a critical potential (E_{pit}) corresponding to the Cl^- concentration required to displace adsorbed oxygen species. In the present study the pitting could be due to the above-mentioned phenomenon occurring in the presence of Cl^- in the pits or could be due to unstable NiO[39] which undergoes dissolution beyond point E. EDX analysis (Fig. 6b) performed on the SEM micrograph in Fig. 6a established the presence of Cl^- and O in this area in region F at the end of

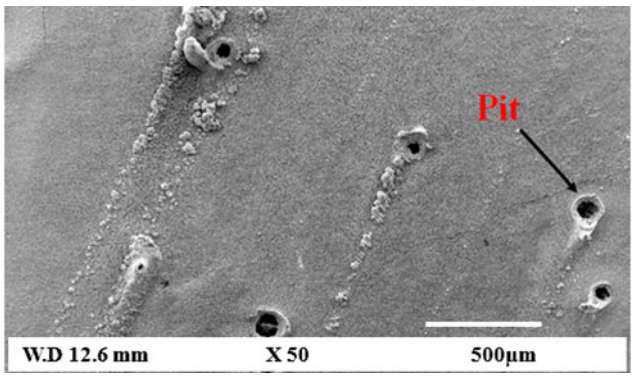

Fig. 5. SEM micrograph showing the pitting corrosion of Sn-1Ag-0.5Cu-0.5Ni solder alloy polarized to the region between E and F during the anodic excursion of the scan.

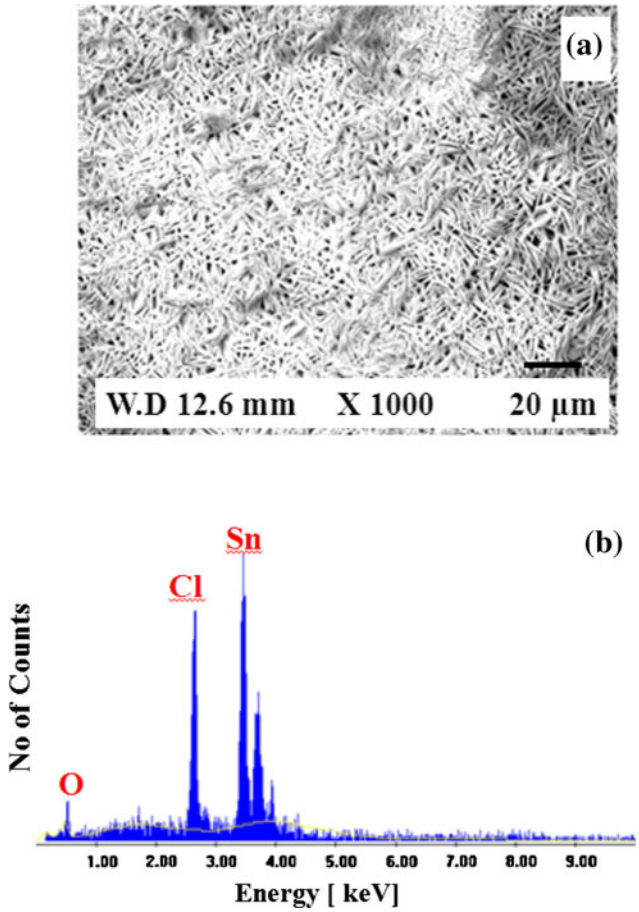

Fig. 6. (a) SEM micrograph obtained for Sn-1Ag-0.5Cu-0.5Ni solder alloy after the completion of the polarization experiments and (b) EDX spectrum.

the polarization experiment. The SEM micrograph for Sn-1Ag-0.5Cu-0.5Ni solder alloy polarized to +100 mV (point F) shown in Fig. 6a reveals a mixture of compact, sheet-like structures with many pores and openings caused by the presence of Cl^- on the outer surface of the solder alloy.

The formation of tin oxyhydroxy chloride has been postulated in the literature by the following equation:[40]

$$3Sn + 4OH^- + 2Cl^- \rightarrow Sn_3O(OH)_2Cl_2 + H_2O. \quad (10)$$

Hence, from the morphological investigations of the polarized Sn-1Ag-0.5Cu-*X*Ni solder alloys, it can be stated that Sn-1Ag-0.5Cu-0.5Ni solder alloy undergoes significant corrosion (Fig. 6a) in comparison with the four-element solders containing 0.05 wt.% and 1 wt.% Ni. Also, the noble E_{pit} values exhibited by the Sn-1Ag-0.5Cu-0.05Ni and Sn-1Ag-0.5Cu-1Ni solders indicate an improvement in the passivity and corrosion resistance as compared with Sn-1Ag-0.5Cu-0.05Ni solder.

Formation of Sn Whiskers

Sn whiskers were observed when Sn-1Ag-0.5Cu-0.05Ni solder alloy was polarized to the end of the passive region D′ (−500 mV, Fig. 1, curve 1) during the anodic excursion of the potential scan. The morphology of the Sn whiskers is illustrated in the SEM micrograph in Fig. 7a. The length of the whisker is found to be around 70 μm. The EDX spectrum in Fig. 7b confirms the presence of Sn in the analyzed area. Figure 8 shows a pair of Sn whiskers of length ranging from 3 μm to 10 μm scattered on the surface of the solder alloy surrounded by a sparse, inhomogeneous distribution of white particles. These white particles correspond to SnO_2 formed at the end of the passive region D as confirmed by the EDX spectrum in Fig. 7b. Auger spectra analysis (Fig. 8c) performed on the surface of the solder alloy also confirmed the presence of Sn and O. Whisker growth is generally caused by local compressive stress and the presence of surface oxides.[41] It has been established that, when oxidation occurs on a Sn surface, there is too little vacancy migration to maintain the gradient necessary for

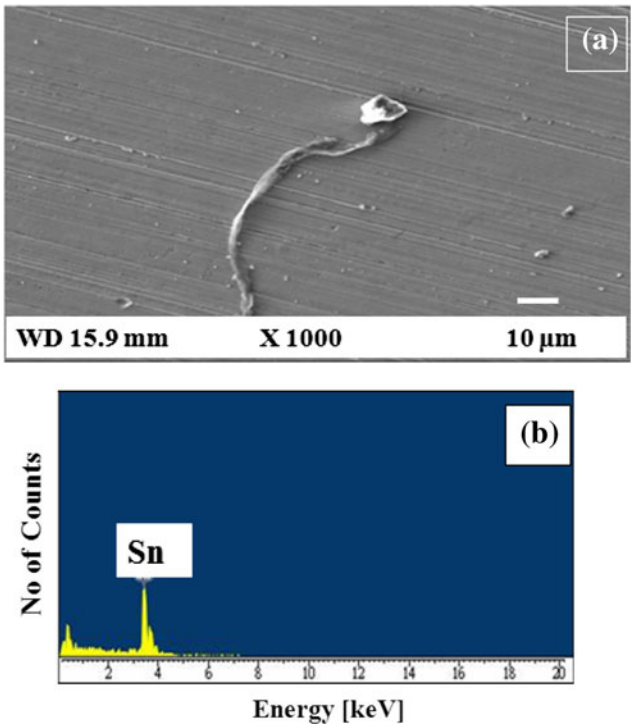

Fig. 7. (a) SEM micrograph demonstrating whisker formation during potentiodynamic polarization of Sn-1Ag-0.5Cu-0.05Ni solder alloy up to the end of the passive region D and (b) EDX spectrum.

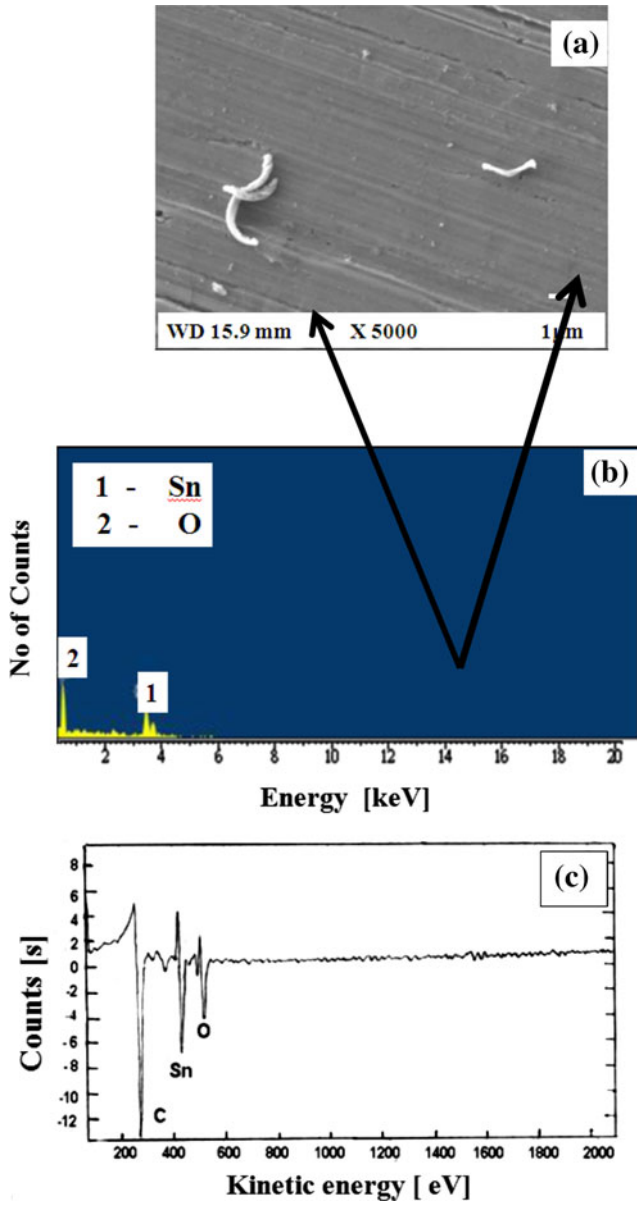

Fig. 8. (a) SEM micrograph showing a pair of Sn whiskers surrounded by nonuniform tin oxide, (b) EDX spectrum, and (c) Auger spectra.

stress relief. Hence, compressive stress is relaxed at broken spots of the Sn surface. This compressive stress increases with time, and in the presence of surface defects, thereby creating the conditions required for breakage through weak spots of the SnO_x layer, at which tin whiskers can then initiate and grow.

Sheng et al.[42] reported that whiskers sprout from weaker spots of the oxide layer on the Sn surface and that the roots of whiskers become localized stress-relief centers. In the present context, the formation of whiskers can be explained by the fact that diffusion of oxygen into the crystal lattice of the Sn-rich phase leads to lattice expansion which is constrained by the surrounding matrix. As a result, compressive stress is created, which extrudes the resulting Sn atoms after oxidation out of the surface of the Sn-rich phase. The diffusion of oxygen is likely governed by the diffusion of oxygen ions through the oxide layer via a vacancy mechanism. The vacancy mechanism process consists of the exchange of oxygen ions and oxygen vacancies. A reaction takes place between two electrons, a vacancy, and an oxygen molecule. This produces an oxygen ion at the oxide surface, which is then able to move through the oxide via a vacancy process.

Since Ni is used as an alloying element in our present study, it might play a role in the formation of whiskers. Several authors[43,44] have opined that Ni plays a role in the formation of whiskers. As reported above, in tin-rich alloy samples with added Ag and Cu, plated over a Ni/Au sublayer, Sn diffuses into Ni at a much higher rate than Ni into Sn. This effect could be responsible for the built-in tensile stress in the lower part of the Sn layer. Hence, results from the present study on whiskers establish that corrosion of Sn-1Ag-0.5Cu-*X*Ni alloy would be due to the development of compressive stress as a consequence of the volume increase due to the formation of corrosion products. Also, buildup of compressive stress due to the formation of Ag_3Sn (Fig. 4a) intermetallic compound formed at the Sn grain boundaries may be proposed as a driving force for whisker growth.

Surface analytical techniques such as AES and SIMS were used to determine the composition of the various corrosion products and oxide films formed on the surface of Sn-1Ag-0.5Cu-*X*Ni solder alloys when subjected to potentiodynamic polarization at different potentials. Figure 9 shows the Auger depth profile for Sn-1Ag-0.5Cu-0.05Ni solder polarized to −750 mV (point C). The figure depicts a significant increase in the atomic concentration of Sn from 20% to 70% with an increase in the sputtering time to 200 s. A further increase in the sputtering time from 200 s to 1200 s also increases the atomic concentration of Sn to 85% in the Auger depth profile. These observations suggest that only a small amount of Sn has oxidized while the rest remains in the sputtered layers and forms the bulk of the alloy. Nevertheless, the atomic concentration of oxygen decreases from 60 wt.% to 20 wt.% with increase in the sputtering time to 200 s. This indicates that most of the oxygen has segregated to the outer surface and has been oxidized in the form of tin oxides. The depth profile results also reveal that the atomic concentration of chloride ions formed on the surface of the solder alloy is 20%, which gradually decreases to 10% with increase in the sputtering time to 200 s and then remains constant with further increase in sputtering time. The presence of chloride ions in certain areas could affect the corrosion behavior of Sn-1Ag-0.5Cu-0.05Ni in two possible ways: either it could result in the dissolution of the passive oxide film in certain areas of the surface of the solder polarized to point D or it would assist in the passivity of the oxide film due to the formation of base salt $SnOHCl_2 \cdot H_2O$.

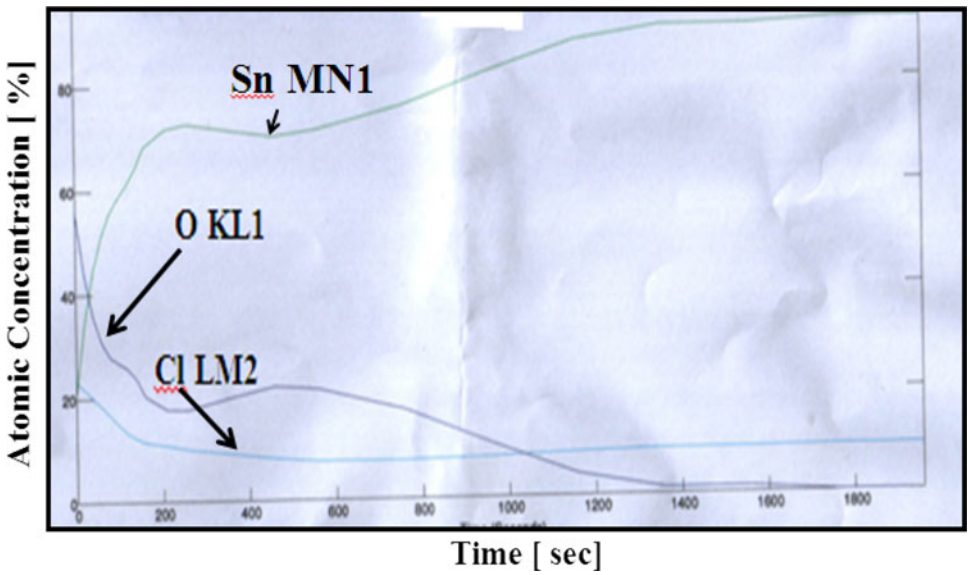

Fig. 9. Auger depth profile analysis for Sn-1Ag-0.5 Cu-0.05Ni solder alloy polarized to −750 mV, point C.

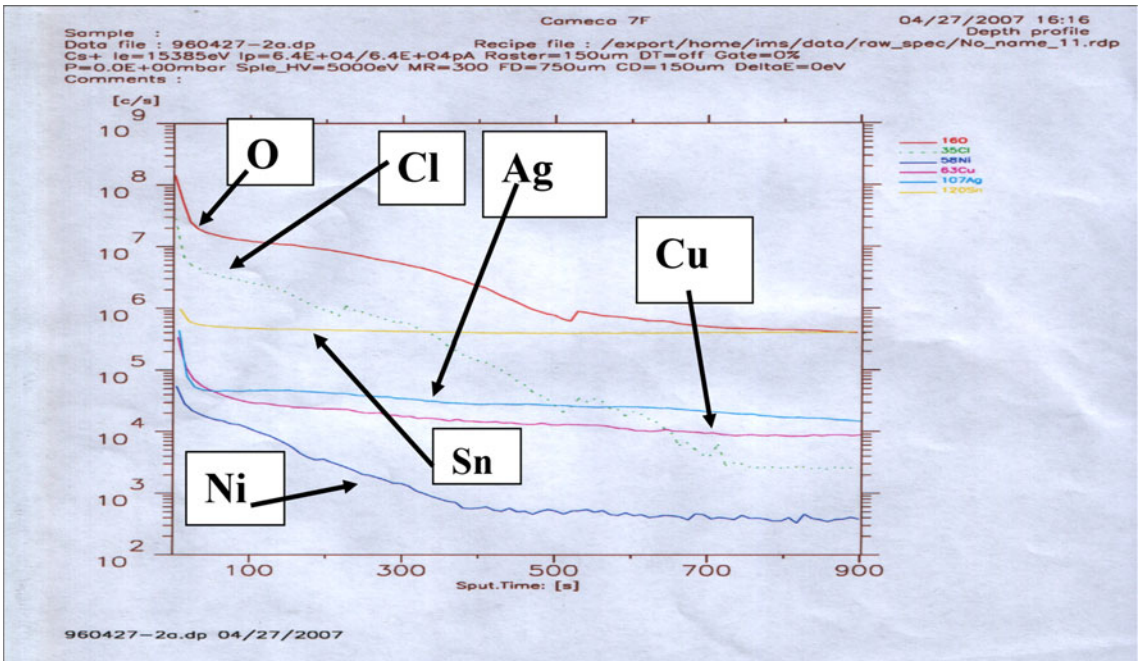

Fig. 10. SIMS depth profile obtained for Sn-1Ag-0.5Cu-0.05Ni solder alloy polarized to −750 mV, point C.

The SIMS concentration profile for Sn-1Ag-0.5Cu-0.05Ni polarized to point C (−750 mV) is presented in Fig. 10. The SIMS spectra establish the presence of a high concentration of oxygen and Sn on the outer surface along with Cl^-, consistent with the Auger depth profile results plotted in Fig. 9. The most notable difference between the Auger depth profile (Fig. 9) and SIMS analysis (Fig. 10) is that SIMS could analyze the presence of other minor elements such as Ag, Cu, and Ni on the outer surface and the sputtered layers. On the other hand, a significant increase in the atomic concentration of Sn (100%) is observed in the Auger depth profile (Fig. 11) when the Sn-1Ag-0.5Cu-0.05Ni solder was polarized to point D (−490 mV, curve 1, Fig. 1). This indicates that the passivation behavior of the solder alloy was due to the possible formation of tin oxides as mentioned earlier. The concentration of oxygen undergoes a significant decrease with increase in the sputtering time to 100 s, indicating segregation of oxygen on the outer surface of the solder alloy. Low concentration of chloride ions would lead to fissures in certain portions of the oxide film, thereby leading to a nonuniform passive film on the surface of the solder alloy.

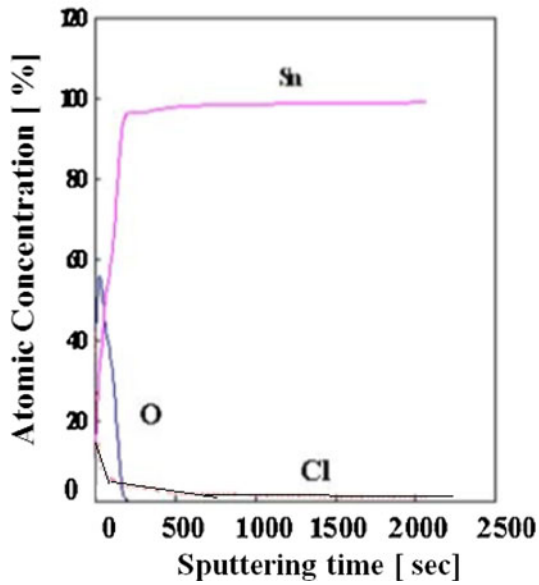

Fig. 11. Auger depth profile analysis obtained for Sn-1Ag-0.5Cu-0.05Ni polarized to point D (−490 mV).

As described earlier, SIMS depth profile (Fig. 12) analysis was performed on Sn-1Ag-0.5Cu-1Ni solder alloy to ascertain the presence of Ni on the surface of the alloy polarized to point E (Fig. 1) during the anodic excursion of the potential scan. The profile results demonstrate that high concentrations of both O and Cl^- are present on the surface of the solder alloy, which seem to gradually decrease with increase in the sputtering time from 50 s to 900 s. Nevertheless, the concentration of Ni undergoes a significant decrease with increase in the sputtering time from 50 s to 300 s, indicating that most of the Ni has segregated to the outer surface of the solder alloy. Hence, the SIMS concentration profile results are consistent with the formation of NiO at point E (−350 mV, curve 3). However, the formed NiO is unstable at this potential (point E) and undergoes dissolution. The presence of a high concentration of Cl^- ions on the outer surface of the solder alloy (Fig. 12) facilitates breakdown and does not allow

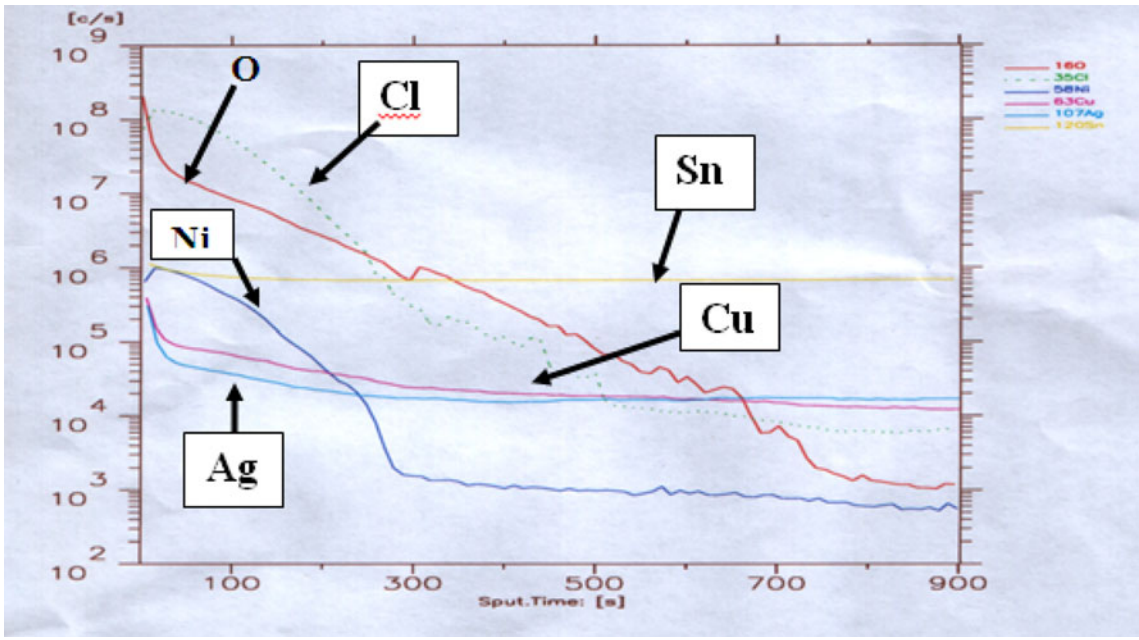

Fig. 12. SIMS depth profile obtained for Sn-1Ag-0.5Cu-1Ni solder alloy potentiodynamically polarized to −350 mV (point E).

the formation of a perfect passive film, thereby inducing pitting corrosion as mentioned above. It may be possible that adsorption of Cl^- ions on the passive layer (SnO and/or SnO_2) can assist pitting on the tin surface due to a chemical reaction between the adsorbed anions and the Sn ions in the oxide film followed by gradual removal of the original oxide and continuous dissolution of the metallic surface, finally leading to the formation of soluble complexes of chlorides of tin. SIMS and Auger depth profile analysis have thus been instrumental in determining the concentration of various elements and their oxides formed on the outer surface of the polarized Sn-1Ag-0.5Cu-*X*Ni solder alloys and the sputtered layers.

CONCLUSIONS

1. Sn-1Ag-0.5Cu-0.05Ni and Sn-1Ag-0.5Cu-1Ni solder alloys demonstrate better passivation abilities and better corrosion resistance properties than the solder alloy containing 0.5 wt.% Ni. These changes are also reflected in the corrosion potential (E_{corr}) of the solder alloys.
2. Auger depth profile and SIMS concentration profiles revealed that oxides of tin play a major role in the formation of the passive film on the surface of the potentiodynamically polarized Sn-1Ag-0.5Cu-0.05Ni solder alloy.
3. Sn whiskers were observed when Sn-1Ag-0.5Cu-0.05Ni was polarized to the end of the passive region in the polarization curve.
4. The mixture of compact sheet/needle-like structures observed in the SEM micrographs is attributed to the formation of tin oxyhydroxy chloride species on the surface of the solder alloy.
5. Significant pitting is noted and a countable number of distinct pits are observed when Sn-1Ag-0.5Cu-0.5Ni solder alloy is polarized to +100 mV during the anodic excursion of the potential scan. The pitting attack is ascribed to competitive adsorption between Cl^- and oxygenated species present at adsorption sites on the oxide covered layer.

ACKNOWLEDGEMENTS

The authors acknowledge the financial support of this study from the National Science Council of the R.O.C. under NSC95-2221-E006-032-MY3.

REFERENCES

1. J. Chen, J. Shen, D. Min, and C.F. Peng, *J. Mater. Sci. Mater. Electron.* 20, 1112 (2009).
2. S.M. Hayes, N. Chawla, and D.R. Fear, *Microelectron. Reliab.* 49, 269 (2009).
3. L. Zhang, S.B. Xue, Z.J. Han, J.X. Wang, L.L. Gao, and Z. Sheng, *Chin. J. Mech. Eng.* 21, 82 (2008).
4. W.C. Luo, C.E. Ho, J.Y. Tsai, Y.L. Lin, and C.R. Kao, *Mater. Sci. Eng. A* 396, 385 (2005).
5. L.C. Shiau, C.E. Ho, and C.R. Kao, *Solder. Surf. Mt. Technol.* 14, 25 (2002).
6. J.Y. Tsai, Y.C. Hu, C.M. Tsai, and C.R. Kao, *J. Electron. Mater.* 32, 1203 (2003).
7. K.S. Kim, S.H. Huh, and K. Sugunama, *J. Alloy. Compd.* 352, 226 (2003).
8. F. Rosalbino, E. Angelini, G. Zanicchi, and R. Marazza, *Mater. Chem. Phys.* 109, 386 (2008).
9. Y.M. Jen, C.K. Fang, and Y.H. Yeh, *IEEE Trans. Compon. Packag. Technol.* 29, 718 (2006).
10. S. Zhang, B. Xue, Y. Chen, Z.J. Han, J.X. Wang, S.L. Yu, and F.Y. Lu, *J. Rare Earths* 27, 138 (2009).

11. Zhang, S.B. Xue, Y. Chen, L.L. Gao, S.L. Yu, Z. Sheng, and G. Zeng, *J. Mater. Sci. Mater. Electron.* 20, 685 (2009).
12. Y.W. Wang, C.C. Chang, and C.R. Kao, *J. Alloy. Compd.* 478, 121 (2009).
13. M.A. Dudek, R.S. Sidhu, N. Chawla, and M. Renavikar, *J. Electron. Mater.* 35, 2088 (2006).
14. J.X. Wang, *Study on Effects of Ce on Properties of Sn-Ag-Cu & Sn-Cu-Ni Solders and Reliability of Solder Joints, Nanjing University of Aeronautics and Astronautics Conference*, Nanjing (2009).
15. K.S. Kim, S.H. Huh, and K. Suganuma, *Microelectron. Reliab.* 43, 259 (2003).
16. F. Rosabino, E. Angelini, G. Zanicchi, R. Carlini, and R. Marazza, *Electrochim. Acta* 54, 7231 (2009).
17. F. Song and S.W. Ricky Lee, *Electronic Components and Technology Conference* (2009), p. 891.
18. U.S. Mohanty and K.L. Lin, *Corros. Sci.* 50, 2437 (2008).
19. C. Hamilton, P. Eng, and P. Snugovsky, Ph.D. Celestica Inc. Toronto, ON, Canada, *Proceedings of International Conference on Lead-free Soldering (CMAP)*, May (2006).
20. U.S. Mohanty and K.L. Lin, *J. Electrochem. Soc.* 153, B319 (2006).
21. U.S. Mohanty and K.L. Lin, *Corros. Sci.* 48, 662 (2006).
22. H. Oulfajrite, A. Sabbar, M. Boulghallat, A. Jouaiti, A. Lbibb, and A. Zrinch, *Mater. Lett.* 57, 4368 (2003).
23. C.M.V. Almeida, B.F. Giiannetti, and T. Rabockai, *J. Appl. Electrochem.* 29, 123 (1999).
24. K. Ogura, *Electrochim. Acta* 25, 335 (1980).
25. M. Mori and K. Miura, *Corros. Sci.* 44, 887 (2002).
26. S. Lu and H.J. Ba, *Sensors* 10, 4145 (2010).
27. H.S. Mohran, A.R. El-Sayed, and H.M.A. EI-Lateef, *J. Solid State Electrochem.* 13, 1279 (2009).
28. F.A. Cotton and G. Wilkinson, *Advanced Inorganic Chemistry*, 3rd ed. (New York: Wiley-InterScience, 1972).
29. S.S. Abd El Rehim, A.M. Zaky, and N.F. Mohamed, *J. Alloy. Compd.* 424, 88 (2006).
30. L.R. Garcia, W.R. Osorio, and A. Garcia, *Mater. Des.* 2, 3008 (2011).
31. S.A.M. Refaey, F. Taha, and T.H.A. Hasanin, *Electrochim. Acta* 51, 2942 (2006).
32. N. Sato and G. Okamoto, *J. Electrochem. Soc.* 110, 605 (1963).
33. B. MacDougall, D.F. Mitchell, and M.J. Graham, *J. Electrochem. Soc.* 132, 2895 (1985).
34. N. Hara and K. Sugimoto, *J. Jpn. Inst. Met.* 47, 39 (1983).
35. K.J. Vetter and H.H. Strechblow, *Localised Corrosion* (Houston, TX: NACE, 1974), p. 240.
36. T. Smialowska, *Industrial Problems Treatment and Control Techniques* (Oxford: Pergamon, 1987).
37. H.P. Leckie and H.H. Uhlig, *J. Electrochem. Soc.* 113, 1262 (1967).
38. J. Horvath and H.H. Uhlig, *J. Electrochem. Soc.* 115, 791 (1968).
39. F. Hunkeler, G.S. Frankel, and H. Bohni, *Corrosion* 43, 189 (1987).
40. D. Li, P.P. Conway, and C. Liu, *Corros. Sci.* 50, 995 (2008).
41. W.J. Choi, T.Y. Lee, K.N. Tu, N. Tamura, R.S. Celestre, A.A. Macdowell, Y.Y. Bong, L. Nguyen, and G.T. Sheng, *52 ECTC Conference Proceedings, IEEE Catalog No. 2, CH3734-5*, San Diego, CA (2002), p. 628.
42. G.T. Sheng, C.F. Hu, W.J. Choi, K.N. Tu, Y.Y. Bong, and L. Nguyen, *J. Appl. Phys.* 92, 64 (2002).
43. A. Skwarek, M. Dhiska, J. Ratajczak, A. Czerhinski, K. Witek, and D. Szwagterczak, *Mater. Sci. Eng. B* 126, 352 (2011).
44. G.T. Galyon and L. Palmer, *IEEE Trans. Electron. Packag. Manuf.* 28, 17 (2005).